

**Test of a theoretical equation of state for elemental solids and liquids**

Eric D. Chisolm, Scott D. Crockett, and Duane C. Wallace

*Theoretical Division, Los Alamos National Laboratory, Los Alamos, New Mexico 87545, USA*

(Received 24 October 2002; revised manuscript received 19 May 2003; published 4 September 2003)

We propose a means for constructing highly accurate equations of state (EOS) for elemental solids and liquids essentially from first principles, based upon a particular decomposition of the underlying condensed matter Hamiltonian for the nuclei and electrons. We also point out that at low pressures the neglect of anharmonic and electron-phonon terms, both contained in this formalism, results in errors of less than 5% in the thermal parts of the thermodynamic functions. Then we explicitly display the forms of the remaining terms in the EOS, commenting on the use of experiment and electronic structure theory to evaluate them. We also construct an EOS for aluminum and compare the resulting Hugoniot curve with data up to 5 Mbar, both to illustrate our method and to see whether the approximation of neglecting anharmonicity etc. remains viable to such high pressures. We find a level of agreement with experiment that is consistent with the low-pressure results.

DOI: 10.1103/PhysRevB.68.104103

PACS number(s): 05.70.Ce, 64.10.+h, 64.30.+t

**I. INTRODUCTION**

Over the last 60 years, numerous models and techniques have been developed for creating equations of state (EOS) for a variety of materials that are valid up to very extreme pressures (tens of Mbar) and temperatures (several eV). In the EOS community at the national laboratories, for instance, we have often used models based on the Mie-Grüneisen EOS together with the Thomas-Fermi or Thomas-Fermi-Dirac model (or one of its modifications) to include the contributions from the electrons (see Ref. 1 for examples). The models usually contain enough independent parameters to adjust the EOS until it correctly reproduces the experimentally measured Hugoniot curve (and perhaps a few other data points), but it is generally an open question how accurate the EOS is away from the Hugoniot curve. In this paper we argue that for one class of materials, elemental solids and liquids, our understanding of the underlying condensed matter Hamiltonian for the nuclei and electrons has grown to the point that we can construct highly accurate EOS from essentially first principles, and we also propose a means for doing so. We also argue that, since the underlying physics is well understood, an EOS derived this way should have the right functional form, even if we are unsure of the values of some of its parameters; thus, if the resulting EOS is shown to be accurate in one thermodynamic region (say, along the Hugoniot curve), then we can be confident that it is roughly equally accurate elsewhere.

In this formalism, the EOS in the solid phase depends on a decomposition of the Hamiltonian due to Wallace (see Chapter 1 of Ref. 2), extending the work of Born<sup>3</sup> to metals as well as insulators; the resulting free energy contains terms describing the harmonic motion of the nuclei about their lattice sites (phonons), thermal excitation of the electrons from their ground state, anharmonic corrections to the nuclear motion (represented as phonon-phonon interactions), and interactions between the electron excitations and the nuclear motion, represented as electron-phonon interactions. (Note that this description is exact; all of the physics contained in the true Hamiltonian of the system is included here. Specific

EOS models usually neglect the anharmonic and electron-phonon terms, arguing that anharmonicity is small and making reference to some form of the Born-Oppenheimer approximation; we will take a somewhat different route, commenting on approximations below.) A recently developed theory of the dynamics of monatomic liquids (see Ref. 4 for a review) uses the same Hamiltonian to derive a liquid free energy which is quite similar to the expression for a solid, with additional terms accounting for the fact that the liquid, as opposed to the solid, traverses many potential valleys and thus sees the boundaries between them. For both phases, the resulting free energies have been compared with experimental data in the low-pressure regime ( $P \leq 100$  kbar), with the following results (Secs. 17–19 and 23 of Ref. 2):

(1) Molecular dynamics (MD) calculations of the anharmonic contribution to the entropy of several solids match experimental entropy data to the accuracy of the data themselves.

(2) Low-temperature ( $T \leq 20$  K) calculations of the electron-phonon term for several solids lead to predictions that also match experimental entropy to the accuracy of the data.

(3) Theoretical arguments show that the electron-phonon contribution is entirely negligible except when the electronic contribution dominates the free energy, such as in metallic solids at low temperatures.

(4) For the 27 elemental solids for which accurate data are available from low  $T$  [but not too low; see point (3)] to the melting temperature  $T_m$ , the free energy excluding the anharmonic and electron-phonon terms accounts for the experimental thermal energy and entropy to an accuracy of 5% (in fact, an accuracy of 2% for all but about five materials).

(5) For the six elements in the liquid phase for which accurate data are available at temperatures up to around  $3T_m$ , the effect of neglecting the anharmonic, boundary, and electron-phonon contributions to the energy and entropy is similarly small.

This tells us that at low pressures, we can neglect the anharmonic, boundary, and electron-phonon terms in both the solid and liquid free energy (which happen to be the

hardest terms to calculate), and the resulting thermal energy and entropy are both simple in form and accurate at the 5% level. It is for this reason, not an appeal to the Born-Oppenheimer or other approximations, that we know we can simplify our EOS and what the results of the simplification will be, at least at low pressures.

In this paper we do two things: (1) we describe in more detail this framework for constructing EOS and discuss the theoretical and experimental inputs needed to implement it, and (2) we construct a sample EOS, neglecting anharmonic, boundary, and electron-phonon terms, both to illustrate the method and to discover whether points (4) and (5) above continue to hold in the high-pressure regime. We use aluminum as our sample because of the availability of extensive electronic structure calculations, up to a compression of three, and highly accurate shock Hugoniot curve data, which provide a test of our EOS through both phases to pressures of around 5 Mbar. In Sec. II A we develop the general theory of the solid EOS, and in Sec. II B we do the same for the liquid. In Sec. III A, we construct our sample EOS for Al, comparing it with other EOS work, and in Sec. III B we compute the Hugoniot curve predicted by the EOS and compare it with the experimental data. The results are encouraging. Finally, we review our work, discuss the advantages and disadvantages of this formalism (and how to address the disadvantages), and suggest directions for future development.

## II. GENERAL THEORY

### A. Solid phase

The condensed matter Hamiltonian, decomposed as described above, consists of terms describing the motion of the nuclei in a potential generated by the electrons in their ground state, plus additional terms that lead to the thermal excitation of the electrons and describe their interactions with the nuclear motion. With this Hamiltonian, the Helmholtz free energy per atom for a solid at temperature  $T$  with volume  $V$  per atom takes the form

$$F^s(V, T) = \Phi_0^s(V) + F_{\text{ph}}^s(V, T) + F_{\text{el}}^s(V, T) + F_{\text{anh}}^s(V, T) + F_{\text{ep}}^s(V, T). \quad (1)$$

Here  $\Phi_0^s$  is the static lattice potential (the electronic ground-state energy when the nuclei are fixed at their lattice sites); it depends on the particular crystal structure.  $F_{\text{ph}}^s$  is the contribution from the harmonic motion of the nuclei about their lattice sites,  $F_{\text{el}}^s$  represents the thermal excitation of the electrons when the nuclei are fixed at their lattice sites,  $F_{\text{anh}}^s$  accounts for the anharmonicity of the nuclear motion (which may be represented as phonon-phonon interactions), and  $F_{\text{ep}}^s$  expresses the interactions between the electron excitations and the nuclear motion, represented as electron-phonon interactions. (We emphasize again that this free energy is exact; it includes all of the physics present in the Hamiltonian.) The discussion in the Introduction justifies approximating the solid free energy as

$$F^s(V, T) = \Phi_0^s(V) + F_{\text{ph}}^s(V, T) + F_{\text{el}}^s(V, T), \quad (2)$$

so let us now consider the forms of  $F_{\text{ph}}^s$  and  $F_{\text{el}}^s$  and the parameters on which they depend. The phonon term in the Hamiltonian describes harmonic motion, which leads uniquely to the free energy of lattice dynamics:

$$F_{\text{ph}}^s(V, T) = \int_0^\infty g^s(\omega) \left[ \frac{1}{2} \hbar \omega + \ln(1 - e^{-\beta \hbar \omega}) \right] d\omega, \quad (3)$$

where  $\beta = 1/kT$  and  $g^s(\omega)$  is the distribution of phonon frequencies in the Brillouin zone. (Note that  $g^s(\omega)$  is volume dependent.) Sometimes we require not the full Eq. (3) but only its high- and low-temperature limits, for which we need not the full  $g^s(\omega)$  but only three of its moments, expressed in terms of the characteristic temperatures  $\Theta_0^s$ ,  $\Theta_1^s$ , and  $\Theta_2^s$  defined by

$$\begin{aligned} \ln k \Theta_0^s &= \langle \ln \hbar \omega \rangle_{\text{BZ}}, \\ k \Theta_1^s &= \frac{4}{3} \langle \hbar \omega \rangle_{\text{BZ}}, \\ k \Theta_2^s &= \left[ \frac{5}{3} \langle (\hbar \omega)^2 \rangle_{\text{BZ}} \right]^{1/2}, \end{aligned} \quad (4)$$

where  $\langle \dots \rangle_{\text{BZ}}$  indicates an average over all the frequencies in the Brillouin zone. Then the following limits hold:

$$F_{\text{ph}}^s(V, T) \rightarrow \frac{9}{8} k \Theta_1^s \text{ as } T \rightarrow 0 \quad (5)$$

and

$$F_{\text{ph}}^s(V, T) = -3kT \left[ \ln \left( \frac{T}{\Theta_0^s} \right) - \frac{1}{40} \left( \frac{\Theta_2^s}{T} \right)^2 + \dots \right] \quad (6)$$

at high  $T$ .

The leading term in Eq. (6) describes purely classical nuclear motion, while the series of terms in powers of  $T^{-2}$  are quantum corrections. Keeping only the first quantum correction, the thermodynamic functions derived from Eq. (6) are accurate to 1% at temperatures above  $\frac{1}{2} \Theta_2^s$ .

The electronic excitation free energy  $F_{\text{el}}^s$  can be expressed generally as an integral function of the electronic density of states per atom,  $n^s(\epsilon)$ , and the Fermi distribution

$$f(\epsilon) = \frac{1}{e^{\beta(\epsilon - \mu)} + 1}, \quad (7)$$

where  $\beta$  is still  $1/kT$  and  $\mu$  is the chemical potential. If each atom contributes  $Z$  electrons to the valence bands (notice that  $Z$  is not necessarily the atomic number), with the lowest valence energy set to zero, then  $\mu$  is a function of  $T$  determined by the normalization condition

$$\int_0^\infty n^s(\epsilon) f(\epsilon) d\epsilon = Z. \quad (8)$$

The electronic free energy is then

$$F_{\text{el}}^s(V, T) = \mu Z - \int_0^{\epsilon_F} \epsilon n^s(\epsilon) d\epsilon - kT \int_0^{\infty} n^s(\epsilon) \ln[1 + e^{-\beta(\epsilon - \mu)}] d\epsilon, \quad (9)$$

where  $\epsilon_F$ , the Fermi energy, is the value of  $\mu$  when  $T=0$ . The second term on the right-hand side of Eq. (9) is the subtraction of the electronic ground state energy, which ensures that  $F_{\text{el}}^s \rightarrow 0$  as  $T \rightarrow 0$ . This property makes sense if  $F_{\text{el}}^s$  represents purely thermal excitation of the electrons. (It also avoids double counting of the energy, as the electronic ground-state energy is already represented as  $\Phi_0^s$ .)

We see from this discussion that to evaluate the terms in Eq. (2) for the solid free energy we require three unknown functions:  $\Phi_0^s$ ,  $g^s(\omega)$  (or  $\Theta_0^s$ ,  $\Theta_1^s$ , and  $\Theta_2^s$  if we are concerned only with the high- and low- $T$  limits), and  $n^s(\epsilon)$  (and the associated quantities  $Z$  and  $\epsilon_F$ ). These can be determined in various ways: compressibility data and diamond anvil cell data can be used to construct  $\Phi_0^s(V)$ ; neutron scattering experiments can determine  $g^s(\omega)$  or its various moments at  $P=1$  bar; and for many elements all three of these functions can be computed reliably using electronic structure theory. [Or one could use results from multiple sources in combination, which is often an option with  $\Phi_0^s$  and is basically a necessity with  $g^s(\omega)$ .] One must keep in mind, however, that the accuracy of one's answers will be limited by the accuracy and range of applicability of these functions, regardless of how they are determined.

### B. Liquid phase and two-phase region

According to the theory of liquid dynamics reviewed in Ref. 4, the same Hamiltonian that gave us the solid free energy leads to a similar form for the free energy of a monatomic liquid. In this theory, the region of the many-body potential surface in which the system moves in the liquid phase is dominated by a large number of intersecting nearly-harmonic valleys, called "random" valleys because they correspond to particle configurations which retain no remnant crystal symmetry and which are all macroscopically identical. In particular, the valleys all have the same distribution of normal mode frequencies, and they all have the same depth (which, as in the solid case, is the electronic ground-state energy when the nuclei are fixed at the valley minimum). The resulting liquid free energy per atom is

$$F^l(V, T) = \Phi_0^l(V) + F_{\text{ph}}^l(V, T) + F_{\text{el}}^l(V, T) + F_{\text{ab}}^l(V, T) + F_{\text{ep}}^l(V, T) - kT \ln w. \quad (10)$$

All of the terms correspond to their solid counterparts with the following exceptions.

(1)  $\Phi_0^l$ , now called the static *structure* potential, is the depth of a typical valley in which the liquid system moves.

(2) The normal mode spectrum appearing in  $F_{\text{ph}}^l$  is that of a typical liquid potential valley, not the unique solid potential valley.

(3) The term  $F_{\text{ab}}^l$  includes corrections due both to anharmonicity and to the fact that the potential valleys have boundaries, which the liquid (as opposed to the solid) encounters as it transits from valley to valley.

(4) The extra term  $-kT \ln w$  corresponds to an increase in entropy of  $k \ln w$  per atom; the value  $\ln w \approx 0.8$  is estimated from entropy of melting data of the elements (again, see Ref. 4 for details). In liquid dynamics theory, this term is due to the hypothesis that the number of potential valleys among which the liquid moves is of the order of  $w^N$ , where  $N$  is the number of atoms in the system.

We emphasize that the same Hamiltonian gives rise to both Eqs. (1) and (10); the differences are that the potential is expanded about different equilibrium configurations in the two cases, and that the region of configuration space over which the liquid moves is obviously far larger than the space available to the solid (hence the  $-kT \ln w$  term).

Again making the approximations discussed in the Introduction, our form for the liquid free energy becomes

$$F^l(V, T) = \Phi_0^l(V) + F_{\text{ph}}^l(V, T) + F_{\text{el}}^l(V, T) - kT \ln w, \quad (11)$$

and the additional term  $-kT \ln w$  is fully determined by setting  $\ln w = 0.8$ , as mentioned above. The form of the phonon term is dictated by a central hypothesis of liquid dynamics theory: The motion of the liquid consists of oscillations in the macroscopically similar valleys described above together with occasional *transits* between valleys; the transits are of such short duration that they do not contribute to the thermodynamics to lowest order. Thus we will take  $F_{\text{ph}}^l$  to have the same form as the solid phonon term, Eq. (3), with possibly a different phonon frequency distribution  $g^l(\omega)$ . The electronic excitation term for the solid was derived using only the assumption that the electrons are thermally distributed over the available states using Fermi statistics; all of the information about the configuration of the nuclei is contained in the density of states. Hence,  $F_{\text{el}}^l$  also takes the same form as the corresponding solid term, Eq. (9), with a density of states  $n^l(\epsilon)$  appropriate for the liquid phase. (What this means is discussed briefly below.)

The liquid and solid EOS together determine the melting temperature as a function of pressure  $T_m(P)$  by the requirement that the solid and liquid Gibbs free energies match along the melt curve, or

$$G^s(P, T_m(P)) = G^l(P, T_m(P)). \quad (12)$$

Once the melt curve is determined, one can use the solid and liquid EOS separately to compute  $V_m^s(T)$  and  $V_m^l(T)$ , the atomic volumes of the solid and liquid at melt as functions of temperature. [Of course, using  $T_m(P)$  one can express  $V_m^s$  and  $V_m^l$  as functions of pressure equally well.]

In the case  $V_m^s(T) < V_m^l(T)$  for all  $T$ , which we assume here, the computation of the full two-phase EOS ( $F$ ,  $E$ ,  $S$ , and  $P$ ) for any  $V$  and  $T$  proceeds as follows. If  $V \leq V_m^s(T)$  for the given  $T$ , the system is in the solid phase;  $F^s$  is computed as described in Sec. II A, and the other functions follow from

$$\begin{aligned}
S^s &= - \left( \frac{\partial F^s}{\partial T} \right)_V, \\
E^s &= F^s + TS^s, \\
P^s &= - \left( \frac{\partial F^s}{\partial V} \right)_T.
\end{aligned} \tag{13}$$

If  $V \geq V_m^l(T)$ , the system is in the liquid phase;  $F^l$  is computed as described in this subsection, and the other functions follow from the expressions analogous to Eq. (13). If  $V_m^s(T) < V < V_m^l(T)$ , the system is in the two-phase region; defining  $\eta$ , the volume fraction of the system in the liquid phase, by

$$\eta = \frac{V - V_m^s(T)}{V_m^l(T) - V_m^s(T)}, \tag{14}$$

the thermodynamic functions are

$$F(V, T) = \eta F^l(V_m^l(T), T) + (1 - \eta) F^s(V_m^s(T), T),$$

$$E(V, T) = \eta E^l(V_m^l(T), T) + (1 - \eta) E^s(V_m^s(T), T),$$

$$S(V, T) = \eta S^l(V_m^l(T), T) + (1 - \eta) S^s(V_m^s(T), T),$$

$$P(V, T) = - \frac{F^l(V_m^l(T), T) - F^s(V_m^s(T), T)}{V_m^l(T) - V_m^s(T)}. \tag{15}$$

Finally, we note that just as with the solid, to evaluate the terms in Eq. (11) we require three unknown functions:  $\Phi_0^l$ ,  $g^l(\omega)$  (or  $\Theta_0^l$  and  $\Theta_1^l$ , since we are not likely to need the low- $T$  limit), and  $n^l(\epsilon)$ . In contrast to the solid case, these functions are generally not available experimentally. (It is possible that one might be able to compute  $\Phi_0^l$  using liquid compressibility data, but we suspect that this will be very difficult.) However, for many materials these functions should be computable using electronic structure theory, proceeding much as one would in the solid case except that the nuclei would be arranged not in a crystal configuration but in a disordered structure characteristic of a “random” valley in the liquid potential surface.<sup>4</sup> To our knowledge very few such calculations have been attempted; the only ones we are aware of are  $\Phi_0^l$  and  $g^l(\omega)$  at a single volume for liquid sodium in Ref. 5 (the results are referred to in Ref. 4 and a graph of  $g^l(\omega)$  using their results appears as Fig. 1 in Ref. 6). Another function that is sometimes available is the melt curve  $T_m(P)$ , but this curve cannot be chosen independently of the others, since the solid and liquid EOS determine it jointly; but this can be an advantage, since if  $T_m(P)$  is known from experiment, for example, it can be used to compute one of the other needed functions if it is not otherwise available. In fact, this is how we will determine  $\Phi_0^l$  in our example EOS, to which we now turn.

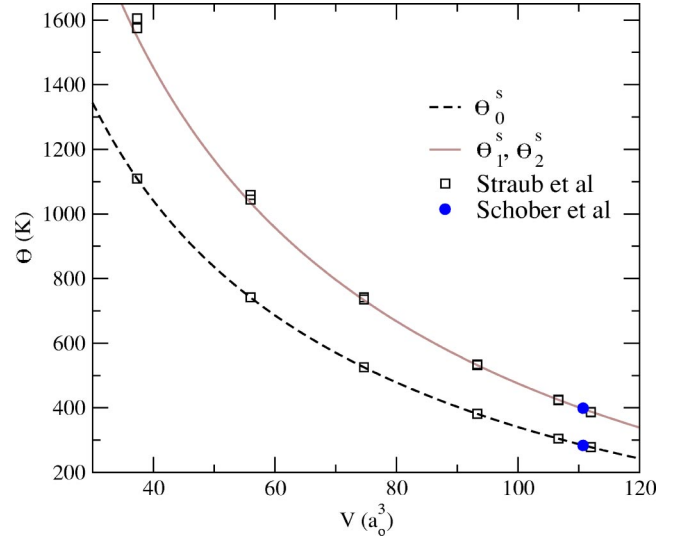


FIG. 1. (Color online)  $\Theta_0^s$ ,  $\Theta_1^s$ , and  $\Theta_2^s$  as functions of atomic volume from the DFT calculations in Ref. 7 and experimental data from Ref. 9. Our functional forms are also shown.

### III. AN EXAMPLE: ALUMINUM

To illustrate the application of the theory we have described, we will now construct an EOS for aluminum, which has been the subject of extensive electronic structure calculations and for which a great deal of high-quality experimental data are available. We will then compare the Hugoniot curve predicted by our EOS with data up to pressures of approximately 5 Mbar; this will tell us whether the approximations we discussed in the Introduction (neglecting anharmonic, boundary, and electron-phonon effects), known to be accurate at low pressures, continue to be reasonable in the high-pressure domain.

#### A. Constructing the EOS

We recall from Sec. II A that the solid EOS requires three functions:  $\Phi_0^s$ ,  $g^s(\omega)$ , and  $n^s(\epsilon)$ . Since we will be testing the EOS by comparison with Hugoniot curve data, we will always be in the high- $T$  region (except for one brief low- $T$  excursion; see below), so we use Eq. (6) for  $F_{\text{ph}}^s$  instead of Eq. (3); this means that we require only  $\Theta_0^s$ ,  $\Theta_1^s$ , and  $\Theta_2^s$  in place of  $g^s(\omega)$ .

To determine these functions, we began by consulting the results of density functional theory (DFT) calculations carried out in the local density approximation by Straub *et al.*<sup>7</sup> They worked with fcc and bcc Al at atomic volumes from  $37a_0^3$  to  $160a_0^3$ , where  $a_0$  is the Bohr radius, corresponding to densities from 8.17 to 1.89 g/cm<sup>3</sup> (the density of Al at 293 K and 1 bar is 2.70 g/cm<sup>3</sup>). Their calculations indicate a  $T = 0$  transition from fcc to bcc at  $51a_0^3$ , corresponding to  $\rho = 5.93$  g/cm<sup>3</sup>, but we will neglect this phase change and treat solid Al as an fcc crystal for two reasons: The DFT calculations themselves suggest that the effect of the phase change on the thermodynamic functions will be quite small; and we know from experiment that the solid-liquid transition on the Hugoniot curve takes place well before reaching the

TABLE I. DFT calculations of  $\Theta_0^s$ ,  $\Theta_1^s$ , and  $\Theta_2^s$  from Ref. 7.

$V(a_0^3)$	$\Theta_0^s$ (K)	$\Theta_1^s$ (K)	$\Theta_2^s$ (K)
111.97	278.09	386.55	387.20
106.65	304.63	423.81	424.86
93.318	381.43	532.00	534.48
74.655	525.01	735.49	741.68
55.991	741.62	1044.7	1058.3
37.327	1109.5	1575.0	1605.4

density of concern (see Sec. III B), so we are confident of our assumption of fcc along the Hugoniot curve until melting. However, this assumption may have an effect on the liquid EOS at high densities, which we will comment on below. (Other electronic structure work, discussed on pp. 89–90 of Ref. 8, suggests the possibility of an hcp phase between the fcc and bcc phases, but as Ref. 8 also mentions, no experimental signature of this phase has been found, so we will proceed under the assumption of a single solid phase.)

Straub *et al.* computed  $\Phi_0^s$  for fcc by fitting their results to a Birch-Murnaghan form,

$$\Phi_0^s(V) = c_0 + V_b \sum_{n=2}^5 \frac{c_n}{n!} \left\{ \frac{1}{2} \left[ \left( \frac{V}{V_b} \right)^{-2/3} - 1 \right] \right\}^n, \quad (16)$$

with coefficients

$$\begin{aligned} V_b &= 106.302a_0^3, & c_0 &= -287.7832 \text{ mRy}, \\ c_2 &= 761.2029 \text{ GPa}, & c_3 &= 1319.036 \text{ GPa}, \\ c_4 &= 13\,661.06 \text{ GPa}, & c_5 &= 50\,315.53 \text{ GPa}. \end{aligned} \quad (17)$$

$\Theta_n^s$  were determined by computing the bulk modulus and four zone-boundary phonons at several volumes, and these results were used to calibrate a pseudopotential model at each volume. The pseudopotential was then used to calculate phonon frequencies throughout the Brillouin zone, allowing the determination of  $\Theta_0^s$ ,  $\Theta_1^s$ , and  $\Theta_2^s$ . Their results are shown in Table I and Fig. 1. (The full set of results was not reported in Ref. 7.) To check these results, Straub *et al.* compared experimental phonon moments for Al at  $T=80$  K and  $P=1$  bar based on Born-von Karmen fits to neutron scattering data<sup>9</sup> with their predictions interpolated to the appropriate atomic volume of  $110.7a_0^3$ . The experimental points, also shown in Fig. 1, are in very good agreement with their calculations; hence, these results for  $\Theta_n^s$  are acceptable for use in our EOS without modification. To determine  $\Theta_n^s$  at any volume, we first constructed a functional fit to the  $\Theta_0^s$  points, with the result

$$\Theta_0^s(V) = 2852.69 + \frac{17\,319.9}{V} + 2.336\,67V - 633.858 \ln(V), \quad (18)$$

where  $\Theta_0^s$  is in K and  $V$  is in  $a_0^3$ . Then we noted that according to the DFT results both  $\Theta_1^s$  and  $\Theta_2^s$  approximately equal  $e^{1/3}\Theta_0^s$ , so we made the same approximation using Eq. (18)

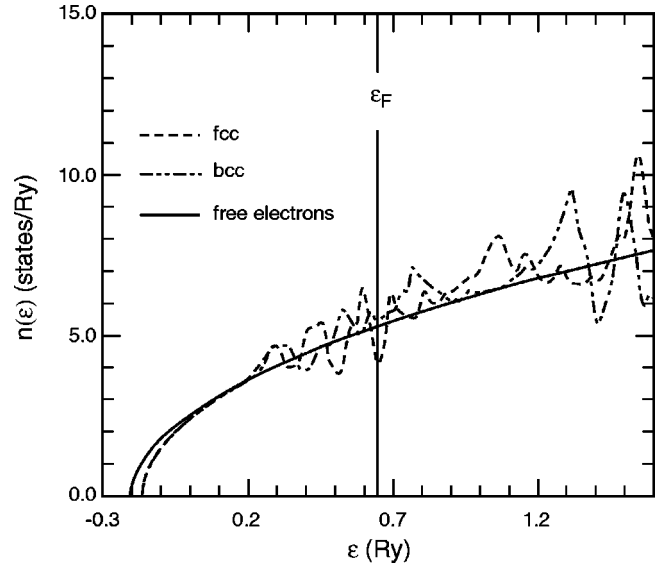


FIG. 2.  $n^s(\epsilon)$  for bcc and fcc Al at atomic volume  $112.0a_0^3$  from the calculations in Ref. 7. The free electron  $n^s(\epsilon)$  at this volume and  $Z=3$  from Eq. (19) is shown for comparison (Ref. 2).

for  $\Theta_0^s$  to determine  $\Theta_1^s$  and  $\Theta_2^s$  at any volume. These functions are also shown in Fig. 1.

The DFT calculations also provided data on the electronic density of states  $n^s(\epsilon)$ . Graphs of  $n^s(\epsilon)$  for fcc and bcc Al at atomic volume  $112.0a_0^3$  (corresponding to  $P=0$  and  $T=295$  K) are shown in Fig. 2, along with the free electron  $n^s(\epsilon)$ , for which

$$n^s(\epsilon) = \sqrt{\frac{\epsilon}{\epsilon_F}} \left( \frac{3Z}{2\epsilon_F} \right)$$

and

$$\epsilon_F = \frac{\hbar^2}{2m_e} \left( \frac{3\pi^2 Z}{V} \right)^{2/3}, \quad (19)$$

at  $V=112.0a_0^3$  and  $Z=3$ . The figure shows that the free electron model is a good approximation for either crystal structure, for electronic excitations to around  $\frac{1}{2}$  Ry. The same match, at a slightly poorer level of approximation and for excitations to around 1 Ry, is found at our smallest atomic volume of  $37a_0^3$ . For all volumes of our study and temperatures up to  $T_m$ , the total electronic excitation contribution to the energy, entropy, and pressure is at most 5%, so the error introduced by using the free electron  $n^s(\epsilon)$  in our calculations is negligible. Making this approximation, the normalization condition from Eq. (8) becomes

$$F_{1/2}(\beta\mu) = \frac{2}{3}(\beta\epsilon_F)^{3/2}, \quad (20)$$

which determines  $\mu$  as a function of  $V$  and  $T$ , and Eq. (9) for the free energy becomes

$$F_{el}^s(V, T) = Z \left( \mu - \frac{2}{3} kT \frac{F_{3/2}(\beta\mu)}{F_{1/2}(\beta\mu)} - \frac{3}{5} \epsilon_F \right), \quad (21)$$

where  $Z=3$ .  $F_n(x)$  are the standard Fermi integrals; their properties are discussed on pp. 332–334 of Ref. 10 and their values for various  $n$  are tabulated in Refs. 11 and 12.

The solid EOS that results from assembling all of these functions is reliable over a large range of volumes and temperatures; however, it is not in perfect agreement with the highly accurate experimental data that are available at low pressures. Specifically, experiments on Al at  $T=0$  and  $P=0$  show that<sup>7</sup>

$$\begin{aligned} V_0 &= 110.6a_0^3, & E_0 &= -249 \text{ mRy}, \\ B_0 &= 79.4 \text{ GPa}, & \frac{dB_0}{dP} &= 4.7, \end{aligned} \quad (22)$$

but the EOS yields  $V_0=107.3a_0^3$ , which is outside the experimental error. Therefore, we chose to make a small correction to our purely theoretical free energy to agree with the experiment. These quantities are obviously determined by the  $T=0$  form of the free energy,  $F_0^s = \Phi_0^s + \frac{9}{8}k\Theta_1^s$  [see Eq. (5)]; since  $\Theta_1^s$  is already in excellent agreement with available experiment, we chose to modify only  $\Phi_0^s$ . To proceed, we noted that the data determine  $P_0$ , the  $T=0$  pressure, in the vicinity of  $V=V_0$  by the relation

$$\begin{aligned} P_0(V) &= P_0(V_0) \\ &+ \left. \frac{dP_0}{dV} \right|_{V_0} (V-V_0) + \left. \frac{1}{2} \frac{d^2P_0}{dV^2} \right|_{V_0} (V-V_0)^2 + \dots \\ &= -\frac{B_0}{V_0} (V-V_0) + \frac{B_0}{2V_0^2} \left( 1 + \frac{dB_0}{dP} \right) (V-V_0)^2 + \dots, \end{aligned} \quad (23)$$

while at higher compressions we have no information to supplement the electronic structure result; so we decided to construct a  $\Phi_0^s$  that correctly reproduces Eq. (23) near  $V_0$  but smoothly interpolates to Eq. (16) at lower volumes. To do this, we computed  $P_0$  at ten volumes between  $110a_0^3$  and  $111.25a_0^3$  using Eq. (23), and we also computed  $P_0 = -\partial F_0^s / \partial V$  using the above form for  $F_0^s$ , with  $\Phi_0^s$  from Eq. (17), at 23 volumes between  $30a_0^3$  and  $41a_0^3$ . We then performed a least-squares fit to these points using an expression similar to the Birch-Murnaghan form, but carried to a slightly higher order; after integrating, adjusting the constant of integration to correctly match  $E_0$  from Eq. (22), and subtracting off  $\frac{9}{8}k\Theta_1^s$ , we had a new  $\Phi_0^s$  given by

$$\begin{aligned} \Phi_0^s(V) &= -1.64615 \times 10^6 + \frac{2.07608 \times 10^7}{V^{2/3}} - \frac{4.61515 \times 10^8}{V^{4/3}} \\ &+ \frac{5.71249 \times 10^9}{V^2} - \frac{5.49998 \times 10^{10}}{V^{8/3}} \\ &+ \frac{3.71978 \times 10^{11}}{V^{10/3}} - \frac{1.66284 \times 10^{12}}{V^4} \end{aligned}$$

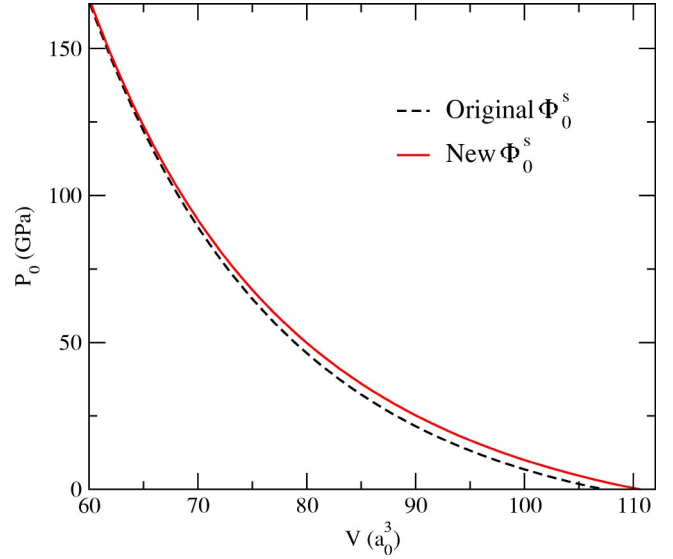


FIG. 3. (Color online) The  $T=0$  pressure-volume relations calculated using the original  $\Phi_0^s$  and the new  $\Phi_0^s$  we constructed. Notice how they differ in the vicinity of  $V=110.6a_0^3$  but then agree more closely at lower volumes.

$$\begin{aligned} &+ \frac{4.41118 \times 10^{12}}{V^{14/3}} - \frac{5.25064 \times 10^{12}}{V^{16/3}} \\ &+ \frac{2.26789 \times 10^7}{V} - 220.716V + 236788 \ln(V), \end{aligned} \quad (24)$$

where  $\Phi_0^s$  is in mRy and  $V$  is in  $a_0^3$ . This  $\Phi_0^s$ , which reproduces the data in Eq. (22) and interpolates smoothly to the DFT curve at higher compressions, is what we use in our EOS instead of Eq. (17). The  $T=0$  pressure-volume curves constructed using both the original and new  $\Phi_0^s$  are shown in Fig. 3.

Our choice of a Birch-Murnaghan–like form was dictated by the fact that the result of Straub *et al.* provides most of our information about the shape of  $\Phi_0^s$ ; so our goal was to preserve that form insofar as was possible, interpolating back to their result as quickly as we could without introducing enough curvature to compromise agreement with  $dB_0/dP$ . This correction to  $\Phi_0^s$  constitutes a small change to the overall EOS; the effect of this change on the Hugoniot curve will be considered in the following section. This modification completes the full solid free energy, so we can now consider the liquid.

For the liquid we need the same three functions that we needed for the solid, and we must also consider the melting curve  $T_m(P)$ . Having chosen to use Eq. (6) for  $F_{\text{ph}}^s$ , we certainly did the same for  $F_{\text{ph}}^l$ , since the Hugoniot curve will obviously enter the liquid region only at rather high temperatures; thus we needed only  $\Theta_0^l$  and  $\Theta_2^l$ . From experiment we know that Al is what is called in liquid dynamics a “normal melting element” (the entropy of melting at constant density is approximately  $0.8k$  per atom), and we argue in Ref. 4 that  $\Theta_0$  in solid and liquid phases of such an element are approxi-

mately equal. (Experimental and computational work supporting this conjecture are also discussed in Ref. 4.) Thus we took the liquid to have the same  $\Theta_0$  as the solid. It is also true that in the liquid,  $T$  is typically much larger than  $\Theta_2^s$  (for example, in liquid Al at normal density  $T \geq 2\Theta_2^s$ ), rendering the first quantum correction to  $F_{\text{ph}}^l$  negligible (roughly 1% at normal density), so even if  $\Theta_2^l$  differs from  $\Theta_2^s$  by 25% or more, the impact on the phonon term will be very small; therefore we also used the same  $\Theta_2$  in the liquid as in the solid.

Since the free electron model approximates the DFT result for  $n^s(\epsilon)$  so well for both fcc and bcc Al (Fig. 2), which correspond to two valleys in the many-body potential surface with rather different structures, we also expect this model to be a good approximation for  $n^l(\epsilon)$ , the density of states for the structure characteristic of a liquid. Since at all volumes and temperatures up to  $5T_m$  (the relevance of this number will appear below), the electronic contribution to the thermodynamic functions does not exceed 25%, the error introduced by the free electron model is still acceptable.

We fixed the only remaining term in Eq. (11),  $\Phi_0^l$ , by the requirement that the Gibbs free energies of the solid and liquid match along the Al melting curve. Boehler and Ross<sup>13</sup> suggested that

$$T_m(P) = 933.45 \text{ K} \left( \frac{P}{6.049 \text{ GPa}} + 1 \right)^{0.531} \quad (25)$$

on the basis of their experimental work up to 80 GPa (0.8 Mbar), and experiments by McQueen *et al.*<sup>14</sup> and Hänström and Lazor<sup>15</sup> and theoretical work by Pélissier<sup>16</sup> suggest that this curve continues to be accurate up to 200 GPa. In the absence of evidence to the contrary, we took Eq. (25) to be valid to higher pressures as needed. (As we will see later, our EOS will assume Eq. (25) no higher than 400 GPa.) We computed  $\Phi_0^l$  as follows: We made a guess for  $\Phi_0^l$  not very different from  $\Phi_0^s$ , and then we used it and Eq. (25) to calculate the difference between the two Gibbs free energies,

$$\Delta G(P) = G^s(P, T_m(P)) - G^l(P, T_m(P)), \quad (26)$$

at several hundred values of  $P$  over the entire pressure range considered in this study. We also calculated the liquid melt volume  $V_m^l(P)$  at each  $P$ . If the rms average of Eq. (26) over all calculated points was not sufficiently small, we used the following easily verified fact: To first order, a small change  $\delta\Phi_0^l$  produces a small change  $\delta G^l(P, T_m(P))$  given by  $\delta G^l(P, T_m(P)) = \delta\Phi_0^l(V_m^l(P))$ . Thus we performed the substitution

$$\Phi_0^l(V) \rightarrow \Phi_0^l(V) + \Delta G(P_m^l(V)), \quad (27)$$

where  $\Delta G$  was computed by Eq. (26) and  $P_m^l(V)$  is the inverse of  $V_m^l(P)$ , and calculated Eq. (26) again. We iterated until the rms average was sufficiently small (less than 0.001 mRy in our case), giving us the needed  $\Phi_0^l$ , which is shown in Fig. 4 along with  $\Phi_0^s$ . We recorded  $\Phi_0^l$  as a list of points,

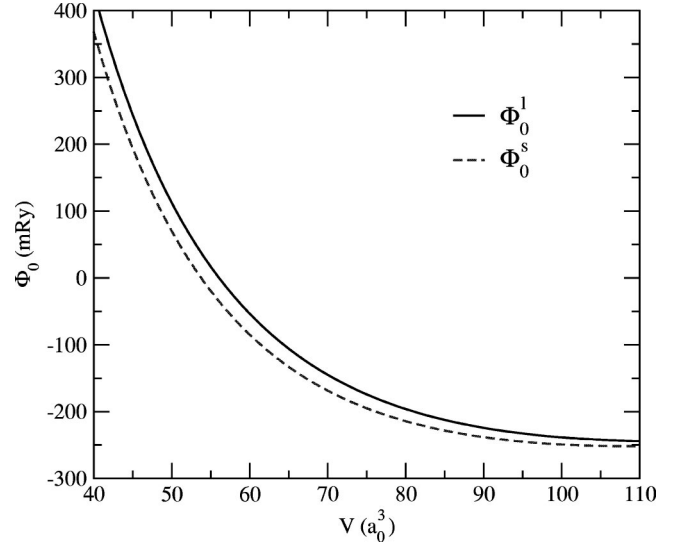


FIG. 4. (Color online)  $\Phi_0^l$  determined by matching the liquid and solid Gibbs free energies along the melt curve.  $\Phi_0^s$  is also shown for comparison.

and we did not create a functional fit for it; instead we used an interpolator to calculate it and its derivative when needed.

It is at this point that the existence of other solid phases in Al, discussed earlier, affects the EOS of the liquid. It is likely that the liquid region borders the fcc crystal only over part of its boundary, beyond which the liquid borders the bcc region or other solid phases. In such a case, at sufficiently high pressures we should use the free energy appropriate for that solid phase, not the fcc free energy, in Eq. (26). This suggests that  $\Phi_0^l$  may become inaccurate beyond densities in the neighborhood of  $6 \text{ g/cm}^3$ , where the  $T=0$  fcc-bcc phase transition occurs. We will take this fact into consideration when we discuss the limits of applicability of the EOS below.

Once we had the full solid and liquid EOS, we then solved Eq. (12) directly to compute  $T_m(P)$ , verifying that we had reproduced the Boehler-Ross curve; our result is shown in Fig. 5, together with the data from Refs. 14 and 15 and some points from Pélissier's theoretical curve. (According to Ref. 14, their data point at 125 GPa marks the onset of melting along the Hugoniot curve. We will comment on this in the following Subsection.)

Now that we have the full two-phase EOS, it is profitable to compare our work with another EOS for Al, due to Moriarty *et al.*<sup>17</sup> These authors also use a full lattice dynamics treatment of the crystal phonons, although they calculate their  $g^s(\omega)$  two separate ways, using both Moriarty's generalized pseudopotential theory (GPT) and a local pseudopotential model with parameters chosen to match solid-phase EOS data. We strongly prefer to rely on DFT results, as we believe DFT has reached such a stage of maturity that it more accurately captures the physics contained in the real Hamiltonian of the system, which as we have emphasized we believe to be understood in sufficient depth that it should underlie all of our work. Second, in their treatment of the

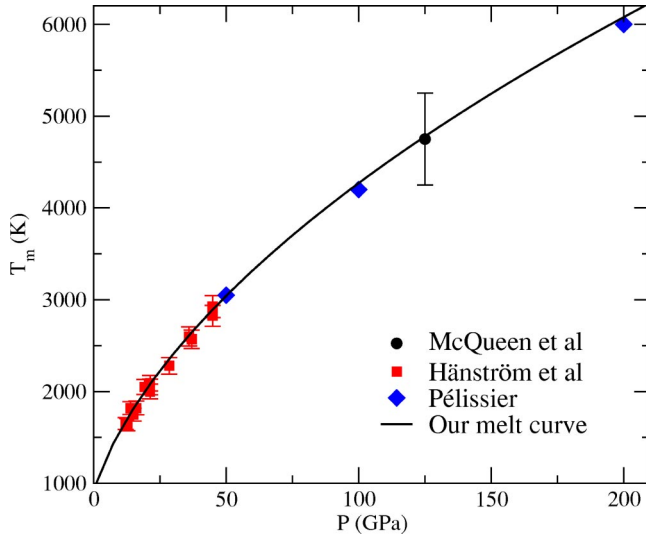


FIG. 5. (Color online) The melt curve  $T_m(P)$  computed from our full solid and liquid EOS [which reproduces the Boehler-Ross curve, Eq. (25)], the experimental data from Refs. 14 and 15, and points from the theoretical curve in Ref. 16.

liquid phase Moriarty *et al.* rely on fluid variational theory, described in detail in Ref. 18, to compute the least upper bound to the “real” liquid free energy (from a liquid Hamiltonian based on pseudopotentials) that can be obtained from the free energy of a reference system; Moriarty *et al.* investigate hard-sphere, soft-sphere, and one-component plasma reference systems before settling on the soft-sphere system as providing the best bound. Based on the investigations summarized in Ref. 4, we claim that we have the actual Hamiltonian of the liquid itself, not a Hamiltonian based on pseudopotential theory; furthermore, this Hamiltonian decomposes naturally into a dominant term that produces a free energy that can be used directly (instead of requiring approximation by the free energy of a reference system) and remaining terms whose contributions to the free energy are known to be small (see the Introduction). The same point we made above for the solid phase applies; we argue that it is a better strategy in developing EOS to try to understand the true Hamiltonian of the system, and then to use it when doing statistical mechanics. Almost inevitably, one must make approximations (which we certainly have done here), but we believe we are in a better position to understand and improve upon them if the physical foundation of the EOS is as solid as we can make it.

Finally, let us make some conservative estimates of the range of applicability of this EOS. Any limits will arise from two sources: the validity of the approximation that  $F_{ab}^l$  is negligible in the liquid (see the Introduction) and the limited ranges over which the functions  $\Phi_0(V)$ ,  $g(\omega)$ ,  $n(\epsilon)$ , and  $T_m(P)$  are known. Let us consider each in turn.

(1) We know from experiment that  $F_{ab}^l$  is negligible when  $T \leq 3T_m$  (again, see the Introduction), and judging from trends in the data we suspect  $F_{ab}^l$  will still be small up to  $T \approx 5T_m$ , but clearly this term must become relevant as the

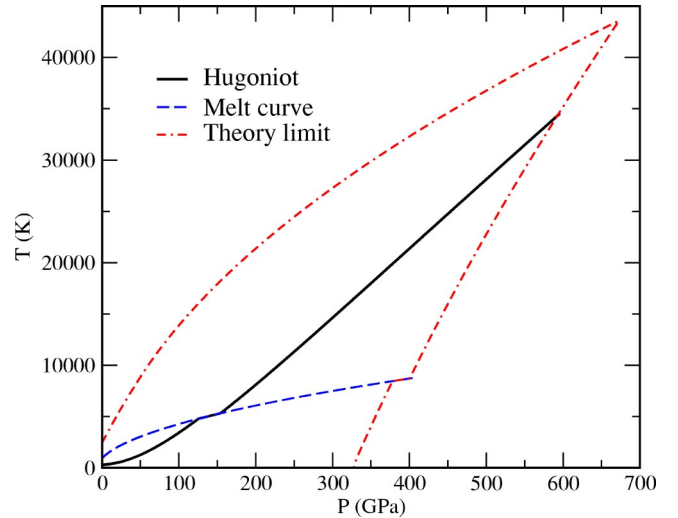


FIG. 6. (Color online) The limits of our EOS, the melt curve, and the Hugoniot curve.

nuclear motion becomes more gaslike. Thus we shall take care with any data at  $\rho$  and  $T$  such that  $T$  approaches or exceeds  $5T_m(\rho)$ .

(2) At densities below approximately  $6 \text{ g/cm}^3$ , we are confident that the solid is in the fcc phase, and the liquid free energy is based on this phase, so we trust the full EOS here. At higher densities, we must be more circumspect; the solid may have undergone a phase transition to bcc, and the liquid EOS at this density may be based on the wrong solid free energy. Further, as we have indicated earlier, Eq. (25) for the melt curve has received independent support only up to 200 GPa, so we must be cautious with the liquid EOS in regions beyond this point. We decided to be brave and accept the melt curve as valid up to 400 GPa; this corresponds to a liquid density of  $6.15 \text{ g/cm}^3$ , and since this is not far from the probable location of the solid fcc-bcc transition, we take it as the density limit of our EOS. (Even if we did not have this concern, we would be restricted to densities below  $8.17 \text{ g/cm}^3$ , where electronic structure results are available.) Also, the free electron approximation to  $n^s(\epsilon)$  has been validated only for  $\epsilon - \epsilon_F$  up to  $1/2 \text{ Ry}$ , or  $6.8 \text{ eV}$ , at low compression and  $1 \text{ Ry}$ , or  $13.6 \text{ eV}$ , at high compression, but at higher temperatures the electronic energy and entropy are sensitive to the details of  $n^s(\epsilon)$  to energies above these limits. We estimated the values of  $T$  that begin to probe the unvalidated region of  $n^s(\epsilon)$  (roughly  $3kT = \epsilon - \epsilon_F$ ), and we found that over our valid density range the  $T = 5T_m$  limit always took precedence. Hence this limit is not relevant for us, but we mention it for completeness, as it may become a concern if the EOS is extended to higher densities.

Figure 6 shows the limits  $\rho \leq 6.15 \text{ g/cm}^3$  and  $T \leq 5T_m$  of the EOS in  $T$ - $P$  space, together with the melt curve and the Hugoniot curve (see the following subsection), while Fig. 7 shows the same three features in  $T$ - $\rho$  space. In this figure, the melt curve becomes a two-phase region, which we will consider in more detail in the following subsection. We are confident that this EOS is valid within these limits, but we don't know how far beyond them the inaccuracies begin to appear;

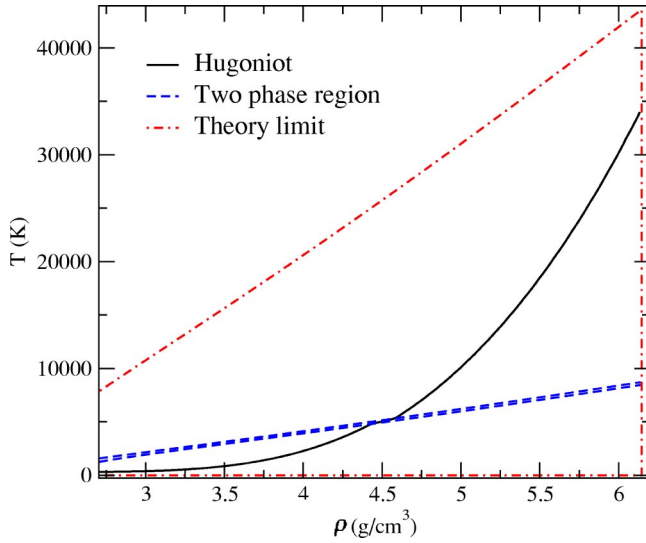


FIG. 7. (Color online) The limits of our EOS, the two-phase region (solid below the region, liquid above), and the Hugoniot curve.

thus we will not be shy about considering data not too far outside this range.

### B. Comparison with Hugoniot curve data

If a shock wave travels at speed  $u_s$  through a sample of material, accelerating its particles from rest to speed  $u_p$  and changing its density, atomic volume, pressure, and internal energy per atom from  $\rho_0$ ,  $V_0$ ,  $P_0$ , and  $E_0$  to  $\rho$ ,  $V$ ,  $P$ , and  $E$ , then (assuming thermal equilibrium before and after the shock) these quantities must satisfy the Rankine-Hugoniot relations,

$$\rho(u_s - u_p) = \rho_0 u_s,$$

$$P - P_0 = \rho_0 u_s u_p,$$

$$E - E_0 = \frac{1}{2}(P_0 + P)(V_0 - V), \quad (28)$$

derived from considerations of mass, momentum, and energy conservation. (It is assumed that the wave is steady and strength effects are negligible.) By solving these equations together with the EOS, which relates  $P$ ,  $V$ , and  $E$ , we can determine the Hugoniot curve, the locus of all possible end states of the shocked material. We used our EOS and Eqs. (28) to compute  $u_s$  as a function of  $u_p$  and  $P$  as a function of  $\rho$  along the Al Hugoniot curve; the results are shown in Figs. 8 and 9 along with the intersection of the Hugoniot curve with the limit of validity of the EOS. Hugoniot curve data from several sources<sup>19–24</sup> are also included. The low-pressure region of the Hugoniot curve is highlighted in Figs. 10 and 11, and the intermediate-pressure region, including the intersections with the phase boundaries, is shown in Figs. 12 and 13.

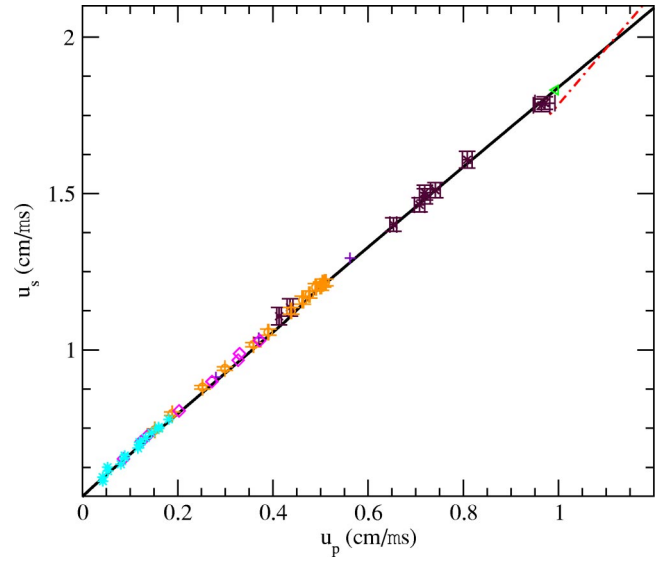


FIG. 8. (Color online) The  $u_s$ - $u_p$  Hugoniot curve for Al predicted by our EOS together with the experimental data from Refs. 19–24. The intersection of the Hugoniot curve with the limit of validity of the EOS (dot-dash line) is also indicated.

Three important considerations in selecting which data to include are (1) the initial densities of the samples, (2) the quality of the experimental technique, and (3) whether the measurements were absolute or relative. All of the available data were taken using Al alloys with densities that differ from the known pure metal value of  $2.70 \text{ g/cm}^3$  (predicted correctly by our EOS); some alloys are as close as  $2.71 \text{ g/cm}^3$ , while others differ much more. Since Hugoniot curves in general are quite sensitive to the initial density, we chose to compare only with the data for which  $\rho_0$  clustered around  $2.71 \text{ g/cm}^3$ . (Thus we used only one data point from

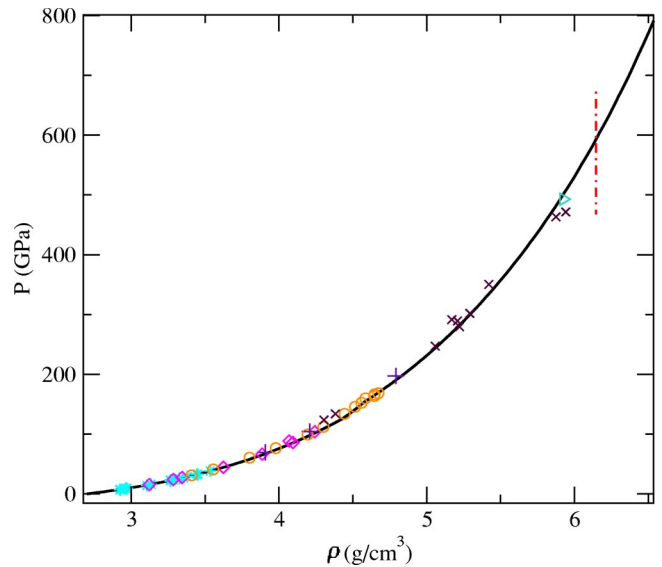


FIG. 9. (Color online) The  $P$ - $\rho$  Hugoniot curve for Al predicted by our EOS together with the experimental data from Refs. 19–24. The intersection of the Hugoniot curve with the limit of validity of the EOS (dot-dash line) is also indicated.

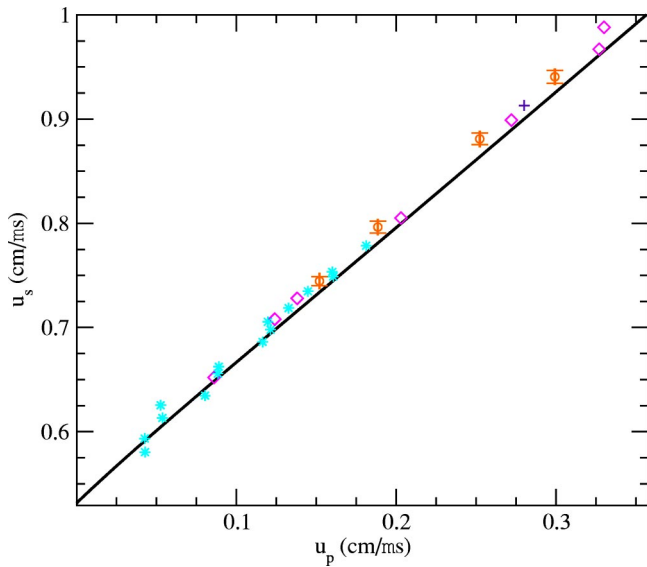


FIG. 10. (Color online) The  $u_s$ - $u_p$  Hugoniot curve in the low- $P$  region, with data from Refs. 19 and 21–23. The  $u_p$  error bars on the circles<sup>23</sup> appear as slightly broadened vertical lines.

Ref. 20, which mainly concerns porous materials. All of the data from the other references were used.) We also avoided sources that gathered data using unusual shock wave geometries (such as Ref. 25), and we also chose not to use the results of indirect or relative measurements, such as Refs. 26–28, preferring to rely on the absolute measurements that are available. Finally, we did not use the few data points available (primarily nuclear driven) that lie very far beyond the limits of applicability of our EOS (but see below).

The theoretical Hugoniot curve compares well with both the  $u_s$ - $u_p$  and the  $P$ - $\rho$  data all the way up to the predicted limit of its validity, at approximately 500 GPa (5 Mbar). More specifically, the theory agrees with experiment at  $P \gtrsim 40$  GPa (Figs. 10 and 11); at 40–125 GPa, the theory falls

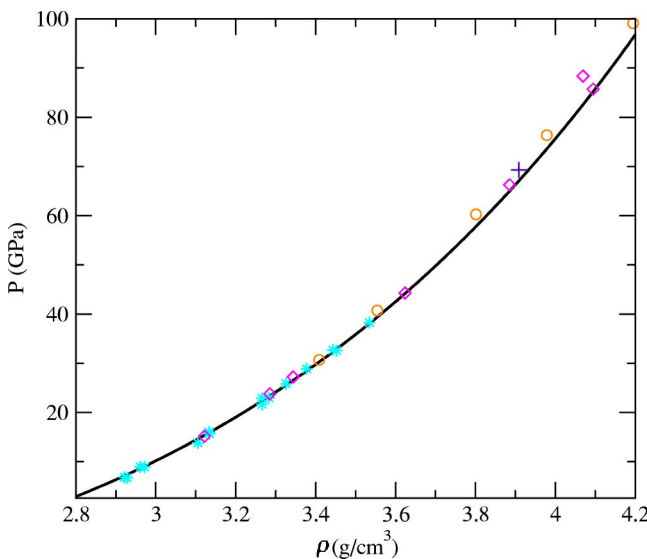


FIG. 11. (Color online) The  $P$ - $\rho$  Hugoniot curve in the low- $P$  region, with data from Refs. 19 and 21–23.

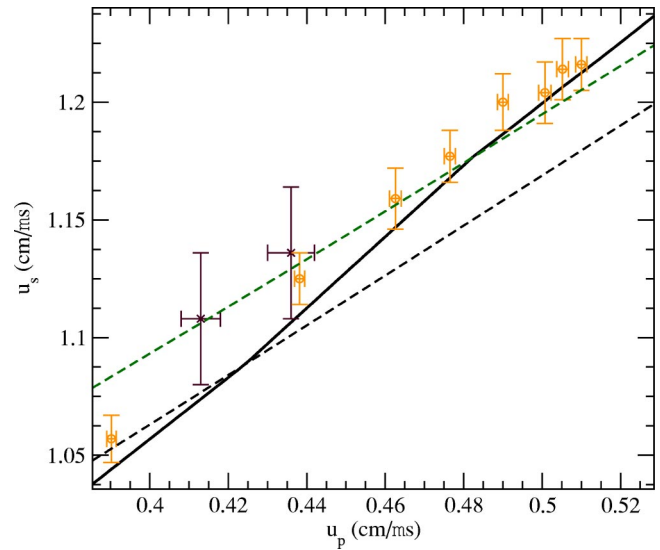


FIG. 12. (Color online) The  $u_s$ - $u_p$  Hugoniot curve in the intermediate- $P$  region, including intersections with the phase boundaries, with data from Refs. 23 and 24.

below the experimental error bars by around 1% at most (Figs. 10–13); and the theory again lies within the experimental error bars through the liquid phase (Figs. 8, 9, 12, and 13). (We recall that given percentage errors in  $u_s$  and  $u_p$  correspond to roughly the same percentage errors in the  $P$ - $\rho$  plane.) The presence of theoretical error only in the solid phase is likely due to strength effects, which are present in the solid but not in the liquid, and which are neglected in our Hugoniot curve calculations. Furthermore, as Fig. 13 shows, we predict that the Hugoniot curve crosses the two-phase region between  $\rho=4.43$  and  $4.58$  g/cm<sup>3</sup>, corresponding to a range in  $P$  from 126 to 156 GPa; this agrees very well with Ref. 14, in which melting was found to occur between 125 and 150 GPa. [We note that Ref. 14 used Al 2024, an alloy

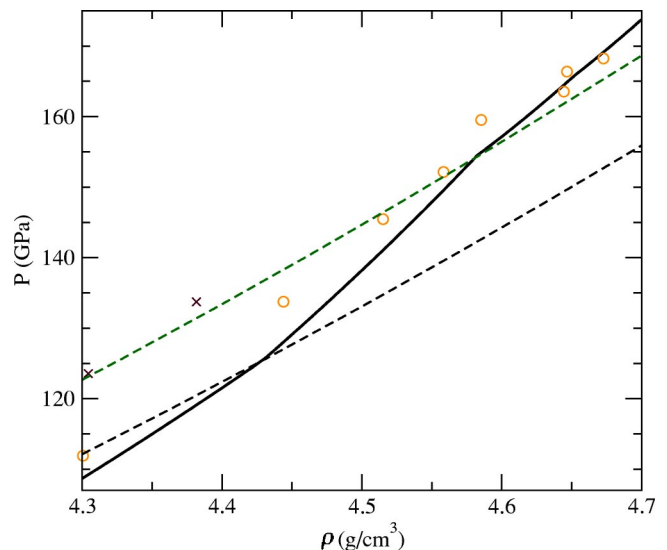


FIG. 13. (Color online) The  $P$ - $\rho$  Hugoniot curve in the intermediate- $P$  region, including intersections with the phase boundaries, with data from Ref. 23 and 24.

whose density is sufficiently different from pure Al that we did not use Hugoniot curve data taken with that alloy in our figures. We consider their melting results because, as we saw in the preceding subsection, their data are consistent with other experiments that did use pure Al.] The correction to  $\Phi_0^s$  from the preceding subsection, shown in Fig. 3, shifts the Hugoniot curve at pressures below 30 GPa, bringing it into excellent agreement with experiment, while at pressures above 60 GPa or so, the effect on the Hugoniot curve is insignificant.

We have also compared our results with data just beyond the EOS limits of validity; the points in Ref. 29 that match our initial density (one of which is a reanalysis of the single point in Ref. 30), lying at about 10 Mbar, fall noticeably below our Hugoniot curve, and their consistency with the very-high-pressure points of Ragan<sup>31,32</sup> strongly suggest that they represent the true Hugoniot curve, which thus falls beneath our prediction at higher pressures. Possible errors in our EOS at such densities include, in what we estimate to be decreasing order of importance, (1) the shift from the fcc to the bcc crystal, with a corresponding change in  $\Phi_0^l$ , as discussed in the last subsection, (2) deviations in the melt curve  $T_m(P)$  from the Boehler-Ross form at higher pressures (the densities of the points in Ref. 29 correspond to melt pressures around 620 GPa according to our EOS), (3) the fact that at such high  $T$  the EOS is probing the high-energy region of  $n^s(\epsilon)$ , and (4) the neglect of the anharmonic and boundary contributions to the liquid EOS ( $T$  is only slightly below  $5T_m$  at these points according to our EOS).

#### IV. CONCLUSIONS

Drawing upon theory developed in Ref. 2, we have described a framework for constructing EOS for elemental solids and liquids, and we have discussed experimental and theoretical results indicating that the framework remains highly accurate at low pressures when certain small effects (anharmonicity, boundaries, electron-phonon interactions) are neglected. After displaying the resulting formulas for the Helmholtz free energy, we considered the information one needs to evaluate them, and we discussed the combination of experiment and theoretical work that could be used to get this information. Finally, as an illustration we constructed an EOS for Al, established its range of validity based on the inputs to the EOS, and compared it with Hugoniot curve data to 5 Mbar; our EOS matched the data to the accuracy we expected based on the low-pressure results.

We consider the primary advantage of this method to lie in the fact that it incorporates into the decomposition of the Hamiltonian a great deal of accumulated knowledge of condensed matter physics both for the solid and liquid phases (for example, the fact that the electronic ground-state energy is the most appropriate potential for the nuclear motion). If we have indeed captured the correct physics (and we expect no new physics to enter until the relativistic domain), then the EOS should have the right functional form, which means that if it is shown to agree with available data, then we have reason to believe that it will be equally accurate in regions

where no data are available; and making predictions where we have no data is the point of having an EOS to begin with. Furthermore, the better the foundation we can build, the better our position for intelligently investigating and controlling our approximations.

This discussion bears on the second goal of this paper, which was to learn whether the approximation of neglecting anharmonic, boundary, and electron-phonon effects remains useful at higher pressures. We already knew, as discussed in the Introduction, that at low  $P$  the anharmonic and electron-phonon terms are small, and we found this from direct calculations; we also knew that for several elements, over a range of  $T$ , at low  $P$  the approximations in question yielded thermal energies and entropies that disagreed with experiments by 5% at most. Our work here has shown that for one material at much higher  $P$  the approximations yield results that match data along a single curve, the Hugoniot curve, to comparable accuracy. Based on our arguments above that the EOS incorporates the correct physics and is thus of the correct functional form, we claim to have shown that this Al EOS is trustworthy throughout its range of validity, for all  $T$  and  $P$ .

The main disadvantage of this method is that it relies on many inputs [ $\Phi_{0,g}(\omega)$ , and  $n(\epsilon)$  for each phase], which may be available only over limited ranges, and each of these limits also restricts the range of validity of the EOS. Our Al example amply illustrates this problem; with a compression range from a little under 1 to just over 2, and a temperature range that reaches only to slightly under 4 eV, this EOS is inadequate for many applications at the national laboratories. We argue, however, that this problem does not indicate a deficiency in the approach; it only underscores the need for many more DFT calculations of these quantities for more materials with ever greater accuracy over ever larger ranges.

In the meantime, though, we would like to be able to say something about elemental solid and liquid EOS at higher compressions. We do know that as density increases, the electrons come to dominate the free energy, and it is also known that TFD correctly describes the electrons in the limit of infinite density. This suggests the following possibility: Construct an EOS using the present techniques to compressions as high as the available experimental or DFT results allow, and then interpolate between these results and the predictions of TFD for higher compressions. This raises an important question: At what pressures does TFD begin to become accurate? Conventional wisdom, usually traced back to Feynman *et al.*,<sup>33</sup> has held that TFD becomes reliable starting at  $P \approx 10$  Mbar, but other work<sup>34</sup> suggests that TFD (or TF in their case, but TF and TFD converge at high pressures) deviates noticeably from electronic structure results until 100 Mbar at least. This suggests that the pressure threshold at which TFD is trustworthy has not yet been adequately established; it would be of great interest to settle this question more definitively.

#### ACKNOWLEDGMENT

This work was supported by the U.S. DOE through Contract No. W-7405-ENG-36.

- <sup>1</sup>S.P. Lyon and J.D. Johnson, Los Alamos Report No. LA-CP-98-100 (unpublished).
- <sup>2</sup>D.C. Wallace, *Statistical Physics of Crystals and Liquids* (World Scientific, Singapore, 2003).
- <sup>3</sup>M. Born and K. Huang, *Dynamical Theory of Crystal Lattices* (Oxford University Press, New York, 1988).
- <sup>4</sup>E.D. Chisolm and D.C. Wallace, *J. Phys.: Condens. Matter* **13**, R739 (2001).
- <sup>5</sup>D.C. Wallace and B.E. Clements, *Phys. Rev. E* **59**, 2942 (1999).
- <sup>6</sup>E.D. Chisolm, B.E. Clements, and D.C. Wallace, *Phys. Rev. E* **63**, 031204 (2001); **64**, 019902 (2001).
- <sup>7</sup>G.K. Straub, J.B. Aidun, J.M. Wills, C.R. Sanchez-Castro, and D.C. Wallace, *Phys. Rev. B* **50**, 5055 (1994).
- <sup>8</sup>D.A. Young, *Phase Diagrams of the Elements* (University of California Press, Berkeley, 1991).
- <sup>9</sup>H. Schober and P.H. Dederichs, in *Metals: Phonon States, Electron States and Fermi Surfaces*, edited by K.-H. Hellwege and J. L. Olsen, Landolt-Börnstein, New Series, Group III, Vol. 13, Pt. a (Springer-Verlag, Berlin, 1981).
- <sup>10</sup>A.H. Wilson, *The Theory of Metals*, 2nd ed. (Cambridge University Press, Cambridge, 1954).
- <sup>11</sup>J. McDougall and F. Stoner, *Philos. Trans. R. Soc. London, Ser. A* **237**, 67 (1938).
- <sup>12</sup>P. Rhodes, *Proc. R. Soc. London, Ser. A* **204**, 396 (1950).
- <sup>13</sup>R. Boehler and M. Ross, *Earth Planet. Sci. Lett.* **153**, 23 (1997).
- <sup>14</sup>R.G. McQueen, J.N. Fritz, and C.E. Morris, in *Shock Waves in Condensed Matter 1983*, edited by J.R. Asay, R.A. Graham, and G. K. Straub (Elsevier, New York, 1984).
- <sup>15</sup>A. Hänström and P. Lazor, *J. Alloys Compd.* **305**, 209 (2000).
- <sup>16</sup>J.L. Pélissier, *Physica A* **128**, 363 (1984).
- <sup>17</sup>J.A. Moriarty, D.A. Young, and M. Ross, *Phys. Rev. B* **30**, 578 (1984).
- <sup>18</sup>N.W. Ashcroft and D. Stroud, in *Solid State Physics*, edited by F. Seitz, D. Turnbull, and H. Ehrenreich (Academic, New York, 1978), Vol. 33, p. 1.
- <sup>19</sup>L.V. Al'tshuler, S.B. Korner, A.A. Bakanova, and R.F. Trunin, *Sov. Phys. JETP* **11**, 573 (1960).
- <sup>20</sup>S.B. Korner, A.I. Funtikov, V.D. Urlin, and A.N. Kolesnikova, *Sov. Phys. JETP* **15**, 477 (1962).
- <sup>21</sup>*LASL Shock Hugoniot Data*, edited by S.P. Marsh (University of California Press, Berkeley, 1980).
- <sup>22</sup>L.V. Al'tshuler, A.A. Bakanova, I.P. Dudoladov, E.A. Dynin, R.F. Trunin, and B.S. Chekin, *J. Appl. Mech. Tech. Phys.* **22**, 145 (1981).
- <sup>23</sup>A.C. Mitchell and W.J. Nellis, *J. Appl. Phys.* **52**, 3363 (1981).
- <sup>24</sup>M.D. Knudson, R.W. Lemke, C.A. Hall, C. Deeney, and J.R. Asay, *J. Appl. Phys.* (to be published).
- <sup>25</sup>I.C. Skidmore and E. Morris, in *Thermodynamics of Nuclear Materials* (International Atomic Energy Association, Vienna, 1962), p. 173.
- <sup>26</sup>L.V. Al'tshuler, N.N. Kalitkin, L.V. Kuz'mina, and B.S. Chekin, *Sov. Phys. JETP* **45**, 167 (1977).
- <sup>27</sup>R.F. Trunin, *Bull. Acad. Sci. USSR, Phys. Ser. (Engl. Transl.)* **22**, 103 (1986).
- <sup>28</sup>B.L. Glushak, A.P. Zharkov, M.V. Zhernokletov, V.Ya. Ternovoi, A.S. Filimonov, and V.E. Fortov, *Sov. Phys. JETP* **69**, 739 (1989).
- <sup>29</sup>V.A. Simonenko, N.P. Voloshin, A.S. Vladimirov, A.P. Nagibin, V.N. Nogin, V.A. Popov, V.A. Vasilenko, and Yu.A. Shoïdin, *Sov. Phys. JETP* **61**, 869 (1985).
- <sup>30</sup>A.P. Volkov, N.P. Voloshin, A.S. Vladimirov, V.N. Nogin, and V.A. Simonenko, *JETP Lett.* **31**, 588 (1980).
- <sup>31</sup>C.E. Ragan, *Phys. Rev. A* **25**, 3360 (1982).
- <sup>32</sup>C.E. Ragan, *Phys. Rev. A* **29**, 1391 (1984).
- <sup>33</sup>R.P. Feynman, N. Metropolis, and E. Teller, *Phys. Rev.* **75**, 1561 (1949).
- <sup>34</sup>W.G. Zittel, J. Meyer-ter-Vehn, J.C. Boettger, and S.B. Trickey, *J. Phys. F: Met. Phys.* **15**, L247 (1985).